OPEN ACCESS
IOP Publishing
Superconductor Science and Technology
Supercond. Sci. Technol. **33** (2020) 114001 (13pp)
https://doi.org/10.1088/1361-6668/abb071

Demonstration of engineering current density exceeding 1 kA mm^{-2} in ultra-thin no-insulation, soldered coil windings using NbTi/Cu wires with CuNi cladding

N Bykovskiy[1], S Kaal[1,2], A Dudarev[1], M Mentink[1] and H H J ten Kate[1,2]

[1] CERN, Experimental Physics Department, Geneva, Switzerland
[2] University of Twente, Faculty of Science and Technology, Enschede, The Netherlands

E-mail: nikolay.bykovskiy@cern.ch

Received 5 May 2020, revised 16 July 2020
Accepted for publication 18 August 2020
Published 18 September 2020

Abstract

The no-insulation, or more precisely, controlled-resistance coil winding method, nowadays being exclusively used for high-temperature superconducting solenoids, has proven its effectiveness for improving quench protection. When considering low-temperature superconductor magnet technology, which is mostly focused on stability and training issues, controlled-resistance insulation windings are directly addressing these aspects as well. Fully soldered coil windings of non-insulated turns can also show superior mechanical properties and feature simplified manufacturing when compared to epoxy impregnated coil windings and are of high practical interest for quasi-stationary magnets provided the related charging time constant can be controlled and kept low enough. For demonstrating the principle feasibility two demonstrator coils were developed using NbTi/Cu wire with CuNi cladding of 1 mm diameter. The wire performance is reported including critical current and n-values at 4.2 K and background magnetic fields from 0 to 9 T, as well as effective transverse resistivity at room temperature and 77 K. Two solenoids with fully soldered windings comprising one layer on a 50 mm bore and three layers on a 100 mm bore, respectively, were manufactured and tested in liquid helium. Their performance is directly compared to data obtained on short wire samples. The drastically enhanced stability of the coils against thermal disturbances allows to avoid any training and enables to operate the coils up, or even slightly beyond, the short-sample critical current, resulting in generated magnetic fields of 2.2 and 3.8 T and time constants of 5 and 55 s, respectively. When initiating a quench deliberately by excessive heating or spontaneously at their limiting currents, the coils entirely switch to the normal state almost instantly, thus requiring no quench protection system. Design, manufacturing and test experiences with the two super stable coils are reported and their use and design constraints for certain applications discussed.

Keywords: NbTi superconductor, no-insulation coil, ultra-thin solenoids, charging time constant, quench propagation

(Some figures may appear in colour only in the online journal)

1. Introduction

Superconducting magnet technology has been successfully employed in the construction of electromagnets with high stored energy, up to the GJ range [1]. Such magnets are operated at relatively low current density J, some tens of A/mm^2, using large amount of stabilizer in the conductor, which is mostly dictated by quench protection requirements [2], and they would even follow $E \sim J^{-6}$ scaling if designed as cryostable [3]. Furthermore, sophisticated and redundant quench detection and protection systems are necessary. On the other hand, a higher current density is favored by economic considerations and overall system efficiency. For instance, advanced detector magnets are often aimed at achieving minimal thickness of coil windings in order to ensure maximum radiation transparency, with applications ranging from particle physics [4] to magnetic spectrometers in space [5]. Hence, magnet design solutions aiming at stored energies beyond 1 MJ, while operating at high current densities of more than 100 A mm^{-2} and addressing stability, as well as mechanical and protection issues, are generally of the high interest.

Coil windings with soldered turns can be effective in dealing with these magnet design aspects. They have been proposed over two decades ago [6] and found promising due to enhanced stability, self-protection feature against quench, and superior mechanical properties. However, parasitic currents across shorted winding turns are present during magnet charging, resulting in a certain lag between operating current and desired magnetic field. The time constant of the delay can be estimated as the ratio of the winding self-inductance over the total transverse resistance, $\tau = L/R$. Hence, achieving a low enough time constant τ is a key consideration in designing such coils and it requires a high transverse resistivity within the coil windings.

In the case of *Re*BCO non-insulated windings, being first reported in [7], the composition of the coated conductors is rather favorable to keep the charging time constant τ within a reasonable limit due to the highly resistive substrate. Nonetheless, using local controlled turn-to-turn insulation may result in the improved performance of multi-layer coils [8]. In contrast to *Re*BCO, direct use of standard NbTi/Cu wires is not appropriate given their very low transverse resistance, except for rather small coils [9]. As a result, local insulation is also investigated for NbTi coil windings [10, 11]. However, the insulation interface is rather weak from the viewpoint of mechanics, which can lead to magnet training [12].

In this work, an alternative solution to restrain the characteristic coil charging time constant τ in fully soldered NbTi/Cu wire based windings is investigated. It is based on using a highly resistive CuNi cladding surrounding the standard NbTi/Cu wire, a technique that may be applied in *Re*BCO coils as well. The CuNi cladding provides a substantial reduction in the charging time constant, improves mechanical properties of the conductor and can directly be pre-tinned. The main properties of the used composite NbTi/Cu/CuNi conductor are provided in the next section, followed by experimental results obtained on two demonstrator coils: a single-layer, 50 mm bore solenoid and a three-layer, 100 mm bore solenoid.

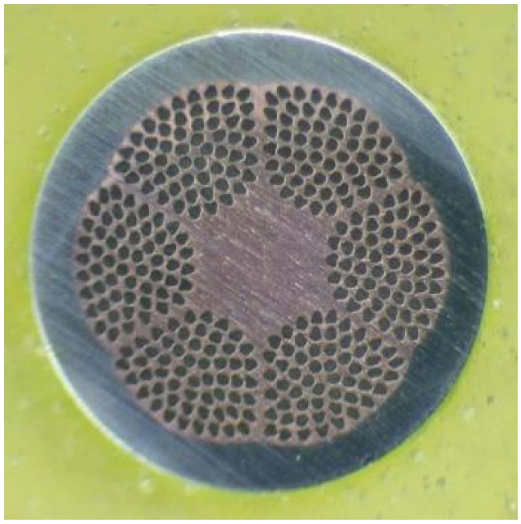

Figure 1. Cross-section of the NbTi/Cu/Cu30Ni conductor.

Table 1. Main parameters of the NbTi/Cu/Cu30Ni conductor.

Parameter	Value
Diameter	1.0 mm
Twist pitch	17 mm
Cu + Cu30Ni to SC ratio	1.7 ± 0.1
Number of filaments	336
Filament size	≈ 30 μm
Thickness of Cu30Ni cladding	≈ 100 μm

Essential design constraints and potential applications are then discussed.

2. Conductor characterization

The requested conductor was manufactured by SuperCon Inc. as a round wire of 1 mm diameter. It is essentially composed of 336 Nb-Ti twisted filaments embedded in a Cu matrix but surrounded by a cladding of Cu30Ni, with the material cross-sections of 0.29 mm^2, 0.21 mm^2 and 0.28 mm^2, respectively, and an RRR along the conductor of 183. In addition, the Cu30Ni conductor surface is pre-tinned using standard eutectic tin-lead solder. The conductor cross-section and its main parameters are summarized in figure 1 and Table1, respectively.

The critical current and n-value of the wire were measured by the manufacturer in a 4.2 K liquid helium bath and in an applied magnetic field ranging from 6 to 9 T. Additional measurements aimed at lower applied magnetic fields in the 0 to 5 T range, were carried out at CERN. Voltage-current transitions were recorded on a short section of the wire, 40 mm long, which was positioned in a uniform magnetic field and immersed in liquid helium. The rather long current transfer length of the sample due to the highly resistive Cu30Ni barrier was addressed, and no current sharing was observed on the short section up until reaching the critical current. The ramp-rate of the transport current was varied from 2 to 50 A s^{-1}, with negligible influence on the test results.

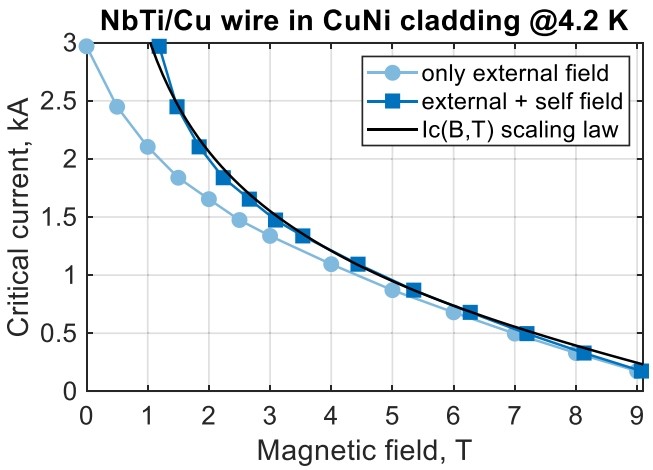

Figure 2. Measured critical current of the NbTi/Cu/Cu30Ni conductor at 4.2 K, shown as a function of external and total magnetic field together with the best fitting $I_c(B,T)$ scaling law of Nb-Ti.

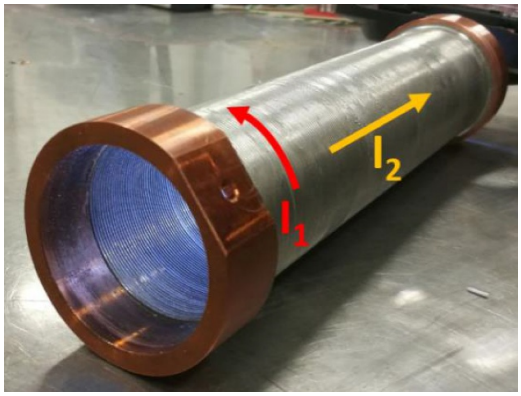

Figure 3. Single layer soldered solenoid with 50 mm bore, as a demonstrator of the thinnest possible coil windings. Note, winding turns visible both from the inner and outer sides of the coil. Directions of current flow along the superconductor, I_1, and transversely to the superconductor, I_2, are also indicated.

The values of the critical current I_c of both datasets are in good agreement, thus the data are presented without any distinction in figure 2 as a function of external and total magnetic field. The self-field contribution was evaluated according to [13], using the average magnetic field produced by the uniformly distributed current in the filamentary region of 0.15 mm inner radius and 0.40 mm outer radius. As a result, the I_c-dependence upon the total magnetic field follows the characteristic $I_c(B,T)$ scaling law of NbTi [14] for T = 4.2 K and using the following fit parameters: $C_0 = 90.3$ kA mm^{-2}, $B_{c20} = 14.5$ T, $T_{c0} = 9.2$ K, $\alpha = 0.57$, $\beta = 0.90$, $\gamma = 2.32$. Note that only C_0 was adjusted, whereas all other parameters are those corresponding to an LHC strand [14]. This scaling is assumed to be valid for temperatures above 4.2 K.

In most of the measurements below 5 T the transition is almost instant, resulting from high operating currents and rather slow data acquisition of few samples per second, thus the n-value is only estimated to be higher than 50. At higher magnetic fields, the n-value is 45 at 6 T, 39 at 7 T and 31 at 8 T, respectively. The critical current density of NbTi at 5 T and 4.2 K is 3.3 kA mm^{-2}.

In order to evaluate the transverse resistivity of the conductor, 100 wires of 50 mm length were stacked horizontally side by side and soldered using eutectic SnPb solder (sample 1) and Rose's metal (sample 2). For the two samples, the total resistance between the first and last wire was measured in air at room temperature and in a liquid nitrogen. The effective transverse resistivity is 440 nΩ.m at RT and 110 nΩ.m at 77 K for sample 1, whereas about 170 nΩ.m at RT and 110 nΩ.m at 77 K for sample 2, respectively. The solder in sample 2 was also very brittle compared to sample 1, with individual wires easily breaking out. Even though uniformity and thickness of the solder was not very well controlled in the samples, the achieved wire stack resistivity is rather high (corresponding τ to be evaluated in the following discussion). For the demonstrator coils, the eutectic SnPb solder was selected.

3. Demonstrator 1: a single-layer, 50 mm bore solenoid

The NbTi/Cu wire with Cu30Ni cladding was used for a single-layer solenoid with 50 mm inner diameter and 200 mm length. The turns are in direct contact and the layer of turns soldered. The winding mandrel was made demountable and was removed after soldering. As a result, the single layer windings of 1 mm total thickness determined by the conductor diameter, is mechanically kept together by solder only, see figure 3.

The effective transverse resistivity of the coil winding ρ is about 170 nΩ.m at RT and 90 nΩ.m at 77 K, lower than that of the 100-wire stack, see section 2, due to the reduced amount of solder. For the given coil parameters (d = 1 mm, D = 50 mm, l = 200 mm) and approximating the coil's self-inductance by that of an infinitely long solenoid, the characteristic time constant can be written as:

$$\tau = \frac{L}{R} \approx \frac{\mu_0 \cdot \left(\frac{1}{d}\right)^2 \cdot \frac{\pi D^2}{4} \cdot l}{\rho \cdot \frac{l}{\pi D d}} = \frac{\mu_0 \pi^2 D^3}{4 \rho d} \approx 4\,s, \qquad (1)$$

where μ_0 is the magnetic permeability of vacuum and the value of ρ is taken at 77 K. Hence, a few percent higher time constant τ is expected at 4.2 K.

Finally, the coil was prepared for measurements at 4.2 K in liquid helium. The summary of the test setup, instrumentation and the main experimental results are presented next.

3.1. Test setup for demonstrator 1

The total voltage including copper terminations as well as the four separate sections can be monitored using five voltage taps installed on the coil, see figure 4. In addition, two single turns of insulated nichrome wire are embedded in the coil, in between the winding turns. They are used as heaters of about 7 Ω resistance to quench the coil deliberately. One hall probe is used to measure the axial magnetic field at the centre of the coil and four pickup coils to evaluate the quench propagation. The

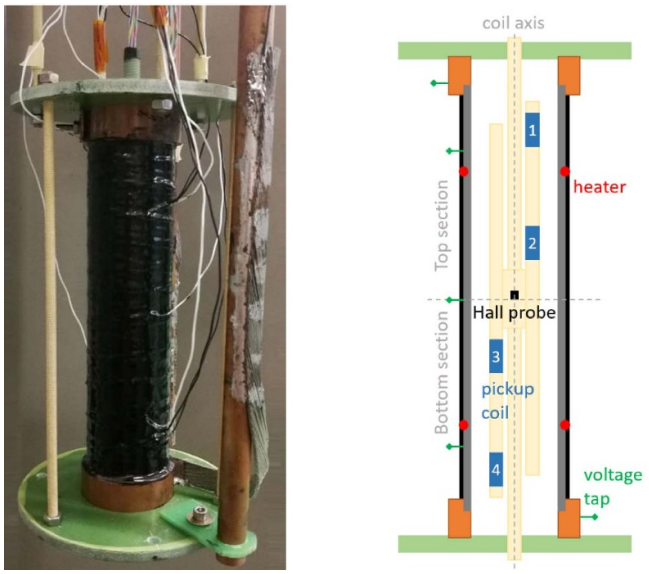

Figure 4. Demonstrator 1: 50 mm bore, 200 mm long solenoid assembled in a test setup (left) and a sketch of the instrumentation showing the position of the hall probe, voltage taps, heaters and pickup coils (right).

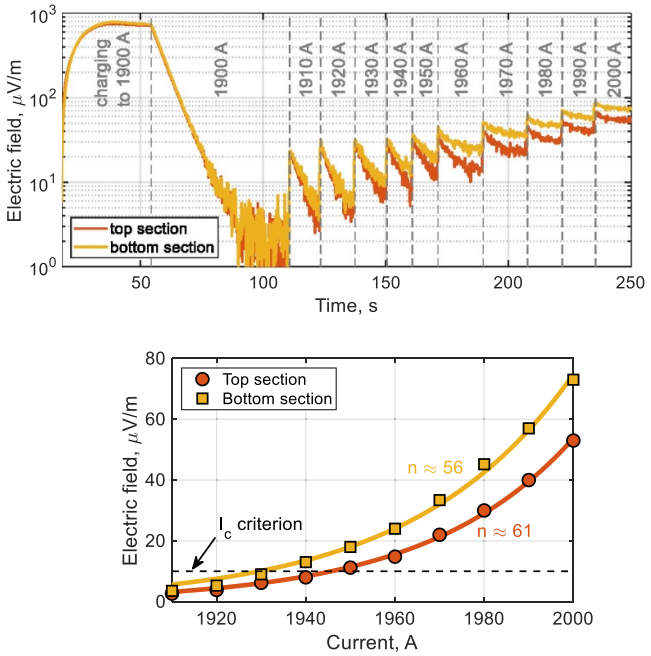

Figure 5. Electric field over the two coil sections measured while ramping operating current in steps. Both inductive and resistive contributions are present in the left picture. Only resistive part, measured at the end of each step, is shown in the right picture as a function of the operating current.

distance between each pickup coil is 60 mm and the pickup coils 2 and 3 are shifted from the coil centre by 30 mm.

As shown in figure 4, the coil is sandwiched in between two G10 disks attached by threaded rods to cryogenic flanges. Because of uncertainty concerning soldering quality of the coil, it was decided to wrap it with a few layers of fiberglass tape wetted with the STYCAST 2850 FT epoxy. This ensures mechanical integrity of the coil for operation at high currents.

High accuracy multimeters operated at low sample rate were used for the data acquisition. They were complemented by a fast data acquisition device in order to trace transient responses of pickup coils in the case of quench.

3.2. Experimental results

The critical current of the coil was measured by ramping the current in steps, using the common Ic criterion of 10 μV m^{-1} as reference. At each step, it takes some time until the inductive voltage contribution vanishes and the resistive part due to flux-flow is actually measured. Figure 5 shows the results obtained over the two coil sections while operating in the transition region from 1.9 to 2.0 kA. It can be seen that the top section of the coil performs slightly better than the bottom one, resulting in a critical current of 1930 A and 1950 A, respectively. The observed transition is quite steep, corresponding to an n-value of about 60. The stationary overcritical operation of the coil suggests that local weak spots are not present in the winding.

Assuming that the current along the superconductor is proportional to the measured axial magnetic field, the time constant can be determined from the magnetic field profile. For example, the measured magnetic field due to a current of 300 A with a ramp rate of 50 A s^{-1} is given in figure 6.

Note that the measured magnetic field is not zero at zero current for this measurement, whereas no offset was present before the first charging. This remnant field can be explained by the superconducting properties of the SnPb solder. At relatively low currents and fields the solder remains superconducting. Upon a field change the induced current in the superconducting SnPb creates the remnant field. At higher currents and during a quench the remnant magnetic field disappears.

The time constant of the coil was measured at various currents and ramp rates. It is presented in figure 7 as a function of the standby current that was reached at a certain value of the ramp rate, varied between 10 and 800 A s^{-1}. The time constant decreases as a function of current, but is independent of the ramp rate. At high currents the time constant settles at 5.6 s. Following equation (1) for the time constant, the transverse resistivity of the coil windings at 4.2 K can be estimated at $\rho = 69$ nΩ.m.

The observed variation in the time constant of a factor 3 to 4 can be understood as follows. The coil's self-inductance L decreases and/or the transverse resistance R increases with increasing current. Both effects are present to a certain extent: at low current, the SnPb solder may become partly superconducting that directly causes a reduction in resistance R, while at high current some current can flow across turns in a steady-state due to the flux creep resistance. Especially when operating at 2 kA, the drop in the time constant down to 3.3 s is caused by the overcritical operation of the coil, see figure 5. In this case, an electrical model of the transverse resistance R in parallel to the coil inductance L and the flux creep resistance (connected in series) should be used instead of an LR model. It is unlikely that the time constant is affected by any magneto-resistive effects. Even though it causes an increase in

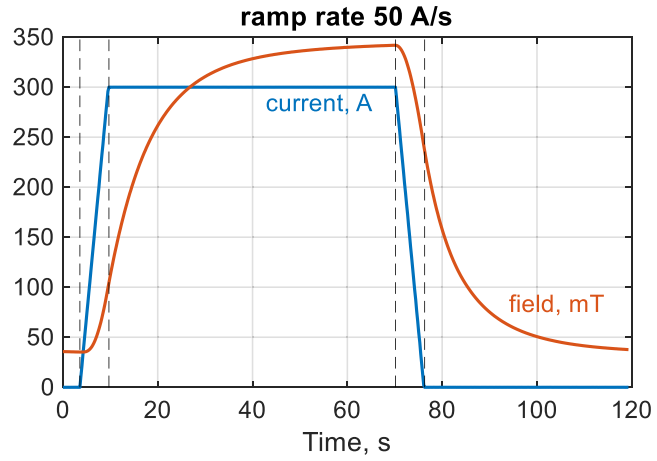

Figure 6. Magnetic field generated at the centre of the coil as a response to the current ramp up to 300 A. The time constant is approximately 10 s and a remnant magnetic field of 30 mT is present due to superconductivity in the SnPb solder.

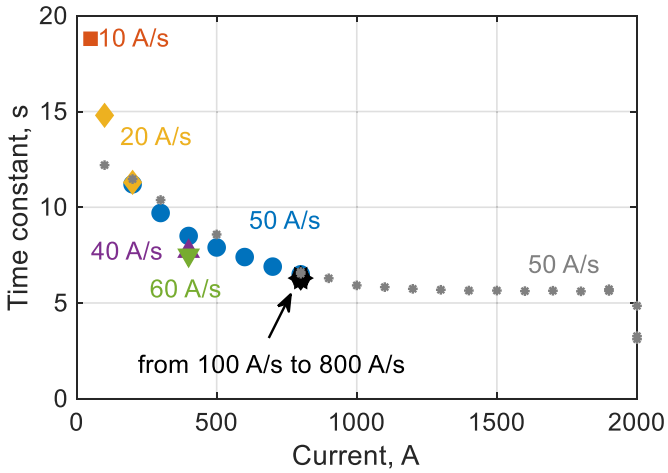

Figure 7. Dependence of the time constant on the operating current for various values of the ramp rate.

the copper's resistivity by a factor 2 for operation at 2 T, the properties of the copper have a negligible effect on the transverse resistivity.

The load-line of the coil obtained from the measurements is compared in figure 8 to an approximation of an infinitely long solenoid and a more accurate simulation accounting for edge effects. The obtained deviation is rather small, but tends to increase at higher currents. The simulated load line intersects the critical surface of the conductor at 2.23 T and 1923 A, which deviates by less than 1% from the measured values, see figure 5. The highest value of magnetic field of 2.27 T was reached at 2 kA. Note that the measured values correspond to steady state operating conditions.

A number of quench tests was performed. Most quenches were deliberately triggered by one of the quench heaters. In addition, one quench occurred near 1.85 kA while ramping at 100 A s^{-1}, but was not recorded, and another one was recorded while operating at 2.0 kA for over 20 s. Figure 9 shows the remarkable quench result for operating the coil at 800 A.

The graph can be divided in five sections:

(a) 0–70 s: The current is ramped up to 800 A at 50 A s^{-1} to charge the coil. The voltage taps show a voltage during the ramp-up. After some time a steady state is reached.
(b) 70–120 s: The heater is fired for about 0.5 s at 12 W. A rather high power is applied to reduce the pulse duration and ensure adiabatic conditions. However, the energy absorbed directly by the winding is rather uncertain. The magnetic field drops sharply to zero and voltages across the voltage taps are observed. After the heater is stopped, the coil recovers. The magnetic field is restored and a steady state is reached again.
(c) 120–160 s: For finding a quench from which the coil cannot recover, the heater power is increased to 24 W for the same duration, however, the coil still recovers.
(d) 160–240 s: Next the heater is fired at 24 W for a twice longer duration, which leads to a thermally irreversible quench. It is observed that the coil tries to recover. First, the magnetic field increases but then sharply drops again. The oscillations continue for a while until magnetic field cannot recover anymore. The bottom section still tries to recover in contrast to the top section, which is at constant voltage of Vtop = 25 mV over the section length l_1 = 75 mm. This also allows to estimate the transverse resistivity at $\rho = (\mathrm{Vtop/I})\ \pi\ \mathrm{D}\ \mathrm{d}/l_1 \approx 65$ nΩ.m, see equation (1).
(e) 240–250 s: The coil is fully discharged in order to bring it back to the superconducting state. As observed from another test at 800 A, the coil also recovers if discharged to 650 A instead of zero current.

Deliberately provoked quenches performed at higher currents with steps of 200 A did not feature self-recovery. Signals from the pickup coils are shown in the left plot in figure 10 for the coil operated at 1 kA and quenched by heater 1, which is located in between pickup coil 1 and pickup coil 2, see figure 4. A certain delay is present among the signals because of quench propagation from the heater location. It is quantified by using a threshold value 0.5 V, leading to 1 ms, 8 ms and 15 ms, respectively.

The delays in response time are summarized in the right plot, which can be helpful to identify the initial point of the quench. As expected, the deliberately provoked quench propagates from top to bottom when heater 1 is fired, and from bottom to top using heater 2. This suggests that the spontaneous quench at 2 kA originated close to the top copper terminal of the coil. Also the propagation velocity of the normal zone can be calculated, which is further discussed in section 5.

4. Demonstrator 2: a three-layer, 100 mm bore solenoid

The fully soldered Nb-Ti windings, first realized in a 50 mm bore single-layer solenoid, were scaled towards 100 mm bore

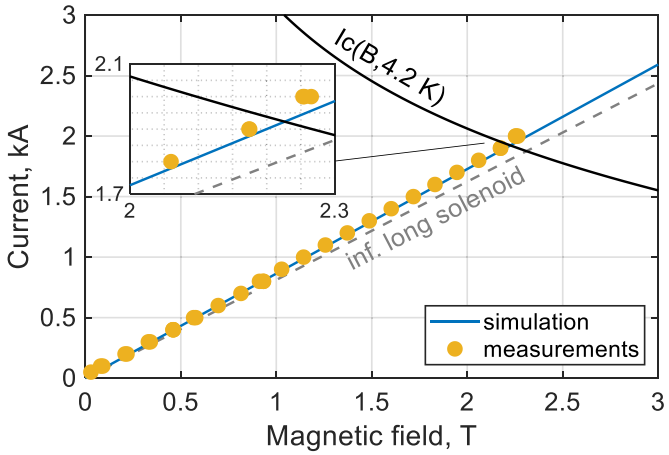

Figure 8. The measured and calculated load lines of the single-layer coil. The critical current of the conductor at 4.2 K and magnified view of its intersection with the load-line are also shown.

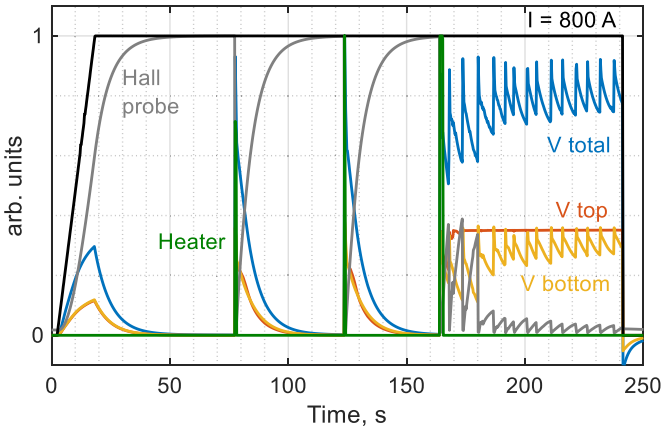

Figure 9. Response of the coil operated at 800 A to three heat pulses. The quenched coil recovers after the first and second pulse, but thermally collapsed after the third one. For clarity, normalized units are used for the coil voltages (using the same factor for Vtotal, Vtop and Vbottom), operating current, generated magnetic field and heat pulses.

and a higher magnetic field, thus increasing the time constant, stored energy, and mechanical stress.

Two winding options can be outlined for multi-layer soldered solenoids: (I) winding layers are internally soldered, insulated from each other and connected in series; (II) winding layers are simply added on top of each other starting from same end of mandrel and then completely soldered without insulation, thus electrically connected in parallel. Option II features simplified manufacturing, a stronger mechanical structure and potentially increased magnet performance due to a current distribution self-adjusting among layers based on the local magnetic field, i.e. the outer layers can carry higher current due to a lower magnetic field. Ideally, each layer should reach its own critical current in a given magnetic configuration and in such case option II using three layers will produce a 10% higher magnetic field than in the case of option I, however the operating current is more than three times higher. Considering an arbitrary number of layers N and neglecting edge effects, the self-inductance and transverse resistance for options I and II and also the single-layer winding are related as follows: $L_I = N^2 L_{II} = N^2 L_1$, $R_I = N^2 R_{II} = N R_1$. Hence, the same time constant is expected for both options, N times higher than that of a single-layer: $\tau_I = \tau_{II} = N \tau_1$.

The second demonstrator coil is based on winding option II comprising three layers of 200 mm length and using the same NbTi/Cu wire with CuNi cladding of 1 mm diameter, see section 2. A closely packed, hexagonal arrangement of strands, featuring up to six contact points among strands, was applied yielding excellent mechanical and thermal properties, a reduced winding width of 2.7 mm and lower excess of SnPb after soldering. Consequently a slightly increased transverse resistance is expected. The time constant can be estimated as $\tau = \tau_1 W/d = 93$ s, where τ_1 is given by equation (1). The winding width W is 2.7 mm and the strand diameter d is 1 mm. The time constant is about 20 times higher than of the single layer solenoid in demonstrator 1, though the self-inductance is rather overestimated by the assumption of an infinite solenoid.

As shown in figure 11, the winding pack geometry and soldering quality have been checked on a dummy sample. Note that some turns are slightly off the groove because the dummy coil was wound with one strand going back and forth along the cylinder axis, which is not the case for the actual winding.

Finally, the 100 mm bore coil was manufactured on a 1 mm thick stainless steel tube, which is in direct contact with the winding. The tube has about a ten times higher resistance along its axis than the windings and the time constant is thus barely affected. A test campaign similar to the one for demonstrator 1 was carried out and the main results are presented here below.

4.1. Test setup for demonstrator 2

Similar to the first coil, the second coil is equipped with the following instrumentation, see figure 12:

- Three voltage taps are soldered on the inner and outer winding layers. They are spaced 75 mm apart and centred at the midplane. Two more voltage taps were added at the copper terminations.
- Two hall probes for measuring the axial magnetic field were installed along the coil axis. One is at the coil centre, the second one is shifted by 50 mm.
- Two heaters were made by a single turn of nichrome wire. They were glued on top of the outer layer using filled epoxy. The heaters are positioned 175 mm apart.
- Eight pickup coils were distributed inside the bore spaced by 30 mm, except pickup coil 4 and pickup coil 5, which are both located at the midplane.

Although the mechanical stress during operation is significantly higher than in the 50 mm bore solenoid of demonstrator 1, there is no risk that the windings can break

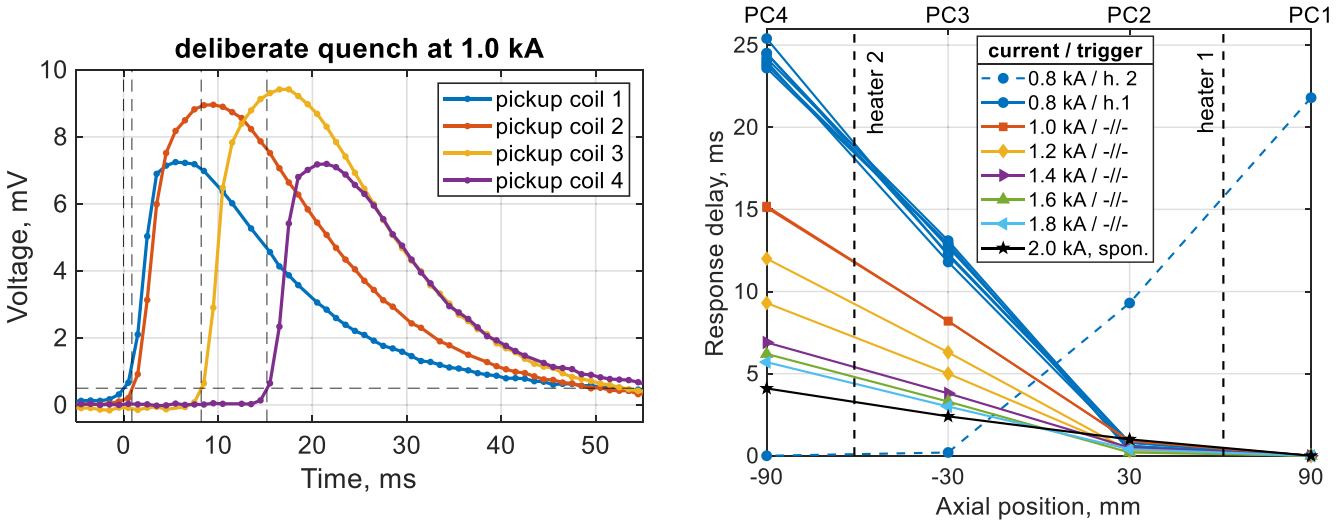

Figure 10. Left: voltage evolution on the pickup coils after the coil is deliberately quenched at 1 kA, showing that it takes about 15 ms to propagate from pickup coil 1 to pickup coil 4. Right: response delay among the four pickup coil voltages for quenches triggered at various operating currents by one of the two heaters and for spontaneous quench at 2 kA.

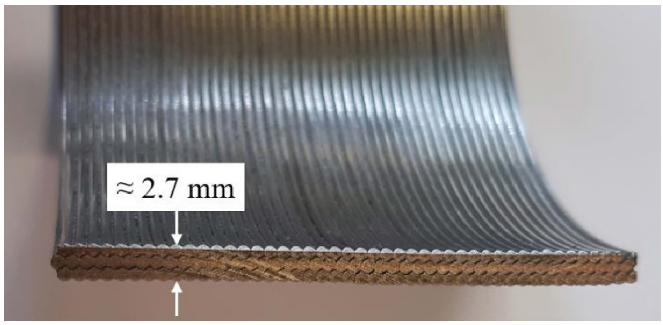

Figure 11. Picture of a three-layer, fully soldered dummy winding after it was cut along the cylindrical axis. Note that each turn is tightly wound, the layers are stacked in the correct configuration according the closely packed hexagonal arrangement of strands, and the total winding thickness is 2.7 mm.

apart in the case of bad soldering due to the presence of the central coil former. No additional mechanical support was added.

The test solenoid is attached by permaglass rods to a cryogenic flange. High accuracy and high acquisition rate devices are used for the measurements of the solenoid in liquid helium.

4.2. Experimental results

The stability of the solenoid is significantly lower than observed on the first single layer solenoid. For instance, operation above 2.5 kA was only possible at ramp rates less than 5 A s^{-1}, otherwise the coil quenched spontaneously. As shown in figure 13, the standby operation current limit was found to be 3.50 kA during the first run, although the coil was also operated for a short time at 3.55 kA and even reached 3.70 kA at 2 A s^{-1}.

The behavior observed may be caused by insufficiently performing superconducting splices connecting the copper terminals of the coil to the current leads. To exclude this, they were reinforced, and a rather marginal improvement was observed in the consecutive test. The coil consistently operates up to 3.60 kA, see figure 13, and up to 3.66 kA when using a ramp rate of just 0.5 A s^{-1}. Nonetheless, the superconducting transition was not recorded. The results of both test runs are discussed here below.

The time constant of the multi-layer coil is determined similarly to what was done for the single-layer solenoid, see figure 14 for the time constant as a function of current. The time constant decreases from 73 s at relatively low currents down to 56 s at 3.50 kA, independent on the ramp rate.

The calculated self-inductance of the coil of 1.70 mH was obtained using a dedicated simulation model. The value was confirmed by measuring the inductive component of the coil voltage during a ramp-up, deviating by less than 2% from the calculated value. Accordingly, the transverse resistivity of the coil at 4.2 K is estimated at 133 nΩ.m, almost twice higher than in the first one-layer coil. Accounting also for the rather weak dependence on the operating current, it is concluded that the impact of the soldering of the turns on the transverse resistivity was substantially reduced in the second three-layer coil.

The load-line of the coil was estimated by calculation assuming that the maximum current in each layer is defined by the peak magnetic field within this layer. Since the magnetic field is produced by currents in all layers at the same time, a self-consistent solution has to be obtained. The calculated critical current is about 3.77 kA, which is shared among the layers as follows: 1.14 kA in the inner layer, 1.28 kA in the middle layer, and 1.35 kA in the outer layer. This configuration generates 4.19 T at the magnet center and 4.23 T, 3.78 T and 3.55 T peak magnetic field within each layer, respectively. Accordingly, about 96% of the ultimate performance was achieved in steady-state operation at 3.60 kA, see figure 13.

The results are presented in figure 15 together with experimental data obtained from the first run. As shown by small

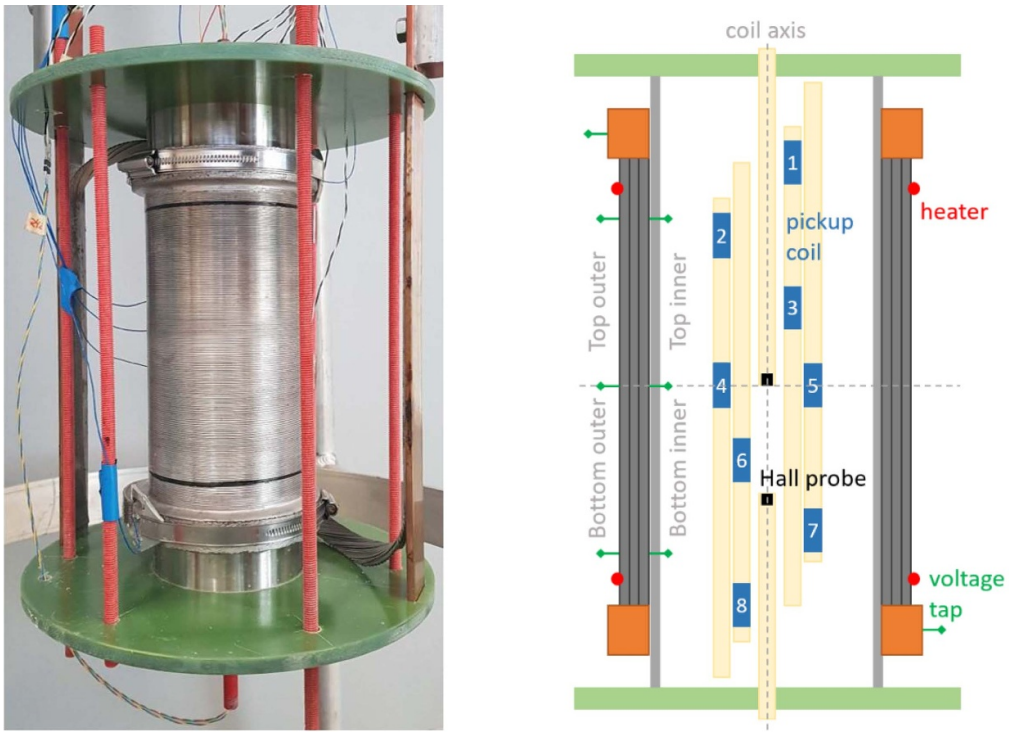

Figure 12. Demonstrator 2 in the test stand: photo of a 100 mm bore, 200 mm long, three-layer solenoid and sketch of the instrumentation.

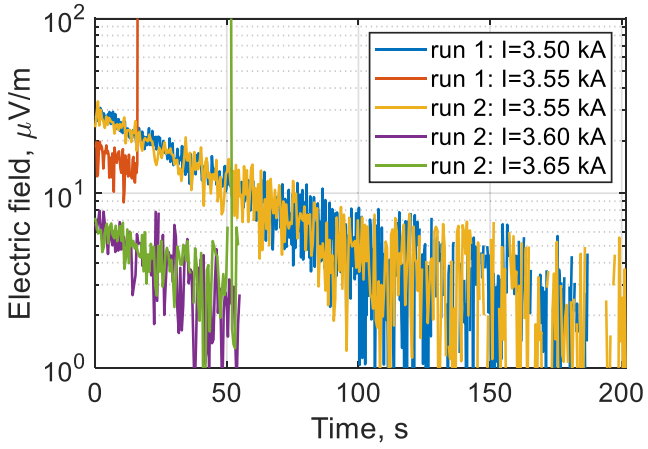

Figure 13. Average electric field over the coil operated at constant current indicated in the legend. The moment of reaching the operating current is set as initial time and exponential decay is then present.

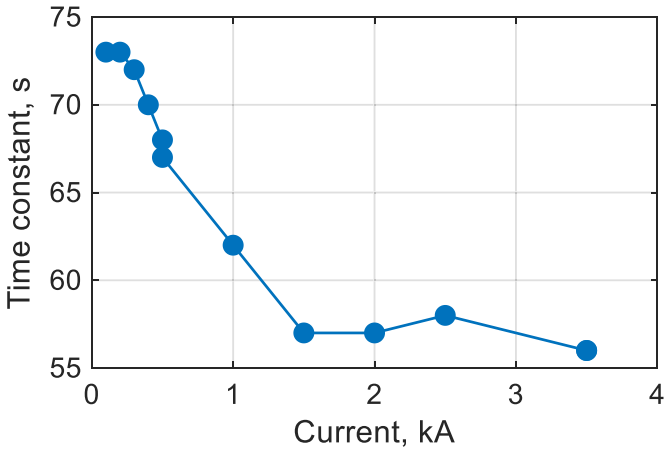

Figure 14. Time constant measured on demonstrator 2, the three-layer coil, as function of operating current.

circles, the ultimate performance of each layer corresponds to the critical current of the conductor at 4.2 K, while the overall performance of 4.19 T center magnetic field at 3.77 kA is even above it.

The magnet generates an impressive 3.66 T in steady state operation at 3.5 kA. At larger currents the magnet would quench spontaneously from time to time, which has occurred at 3.52 kA, 3.55 kA, 3.60 kA and 3.70 kA during the first test run. The maximum achieved magnetic fields are 3.70 T at 3.60 kA and 3.78 T at 3.70 kA, see yellow diamonds in the figure. Although the actual current distribution among layers cannot be obtained, the measured values fairly match the calculated performance, see figure 15.

The operating current is switched off 0.5 s after the coil quenches. However, it only takes some tens of millisecond to reach normal state in the entire coil. For example, one can see in figure 16, the voltage evolution during the spontaneous quench at 3.52 kA. It first starts in the bottom outer section of the coil, see coil sections in figure 12, and reaches both inner sections after about 20 ms, which can be concluded from the corresponding voltage take-off and also from the peak voltage measured across the layers in the magnet's midplane. It takes another 30 ms until the voltages stabilize at about 60 mV along

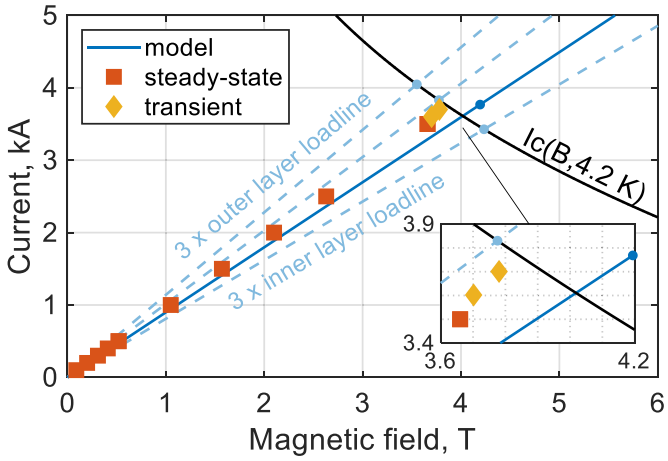

Figure 15. Measured and calculated load-lines of the three-layer solenoid in demonstrator 2. For a direct comparison, the load-lines of individual layers as well as the critical current Ic(B,T) are multiplied by 3.

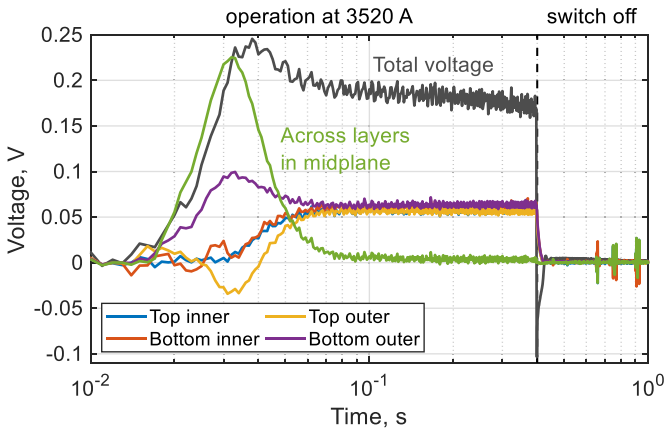

Figure 16. Evolution of the coil voltages during the spontaneous quench at 3.52 kA. The entire coil is in the normal state after about 50 ms and the operating current is switched off after 0.4 s.

the sections and near zero in the transverse direction, thus completely reaching the normal state. Note that a thermal runaway is not present during the quench and the operating current is finally switched off after 0.4 s.

The transverse resistivity can also be estimated from the steady state voltage along the quenched coil sections. It increases weakly with the operating current, from about 170 nΩ.m at 2.5 kA up to 200 nΩ.m for currents above 3.5 kA, and noticeably higher than estimated from the time constant. The impact of temperature on the transverse resistivity might be the origin of the discrepancy as the coil should reach around 100 K temperature during a quench (see next section).

Signals from the pickup coils for the spontaneous quenches at 2.8 kA and 3.6 kA are compared in the left plot of figure 17. In contrast to those of the single-layer solenoid, see figure 10, the signals show a double peak. The first peak can be attributed to the initial quench propagation within a certain layer for a few millisecond, while the second peak after some tens of millisecond indicates that all layers are quenched. Thus, a decrease of the signal after the first peak at relatively low operating currents is an indication that some current redistribution occurs before other layers are quenched.

The delay in response among the pickup coils was investigated using the voltage threshold of 1 V, see figure 17. As expected, profiles obtained from the deliberate quenches indicate locations of the corresponding heaters. In the case of spontaneous quenches at relatively low currents and high ramp rates, one of the pickup coils 3 to 6 reacts first, thus suggesting that the quench origin is near to the coil mid plane. For those obtained at higher current and low ramp rates, pickup coil 1 was always responding first. As mentioned previously, the top splice to the superconducting coil was expected to be a weak spot, but after re-enforcement no improvement was observed in the second run.

Next, the quench propagation velocity is estimated from the slope of the response delay curves and compared to the case of the single-layer coil.

5. Discussion on charging time, quench propagation and hot spot temperature

The performance of the two coils is fairly in line with a simple LR simulation model. The generated magnetic field follows an exponential behavior with time constant τ, defined as the ratio of the coil self-inductance over the transverse resistance. An extensive study of a proper simulation model addressing current sharing, power and energy losses is provided in [15]. In addition, one can express the total time required to reach the targeted magnetic field as follows:

$$t = \tau \ln \frac{\tau\left(e^{t_0/\tau} - 1\right)}{t_0 \varepsilon} \overset{\varepsilon=0.01,\, t_0 \sim \tau}{\rightarrow} \approx 5\tau \qquad (2)$$

where the operating current is ramped linearly from 0 to I_0 with ramp rate α and $t_0 = I_0/\alpha$. Hence, it typically takes about 5τ to reach $(1–\varepsilon) = 99\%$ of the total current in the superconductor. Note that reducing t_0 is not efficient to obtain a lower t. Considering the instant charge to I_0 as the limiting case, one would still need to wait $t = \tau \ln 1/\varepsilon$ to reach $(1–\varepsilon)$ of the desired magnetic field and the total energy released in the transverse resistance is then increased up to the stored magnet energy.

A rather high transverse resistivity was obtained, especially on the second coil in the range of 100 to 200 nΩ.m. Taking into account the conductor composition, see figure 1, it is dominated by the Cu30Ni resistivity of about 400 nΩ.m. Thus, the effective transverse resistivity of the conductor can simply be estimated as ρ 2 t/(d—2 t) ≈ 100 nΩ.m, where d is the conductor diameter and t the thickness of the Cu30Ni cladding. Increasing the transverse resistivity by using a different solder is not planned, given that the SnPb solder gave favorable mechanical performance.

Soldered-turns based coils can actually be charged faster than predicted by equation (2) by overshooting the target operating current. Based on the control methods proposed in [16],

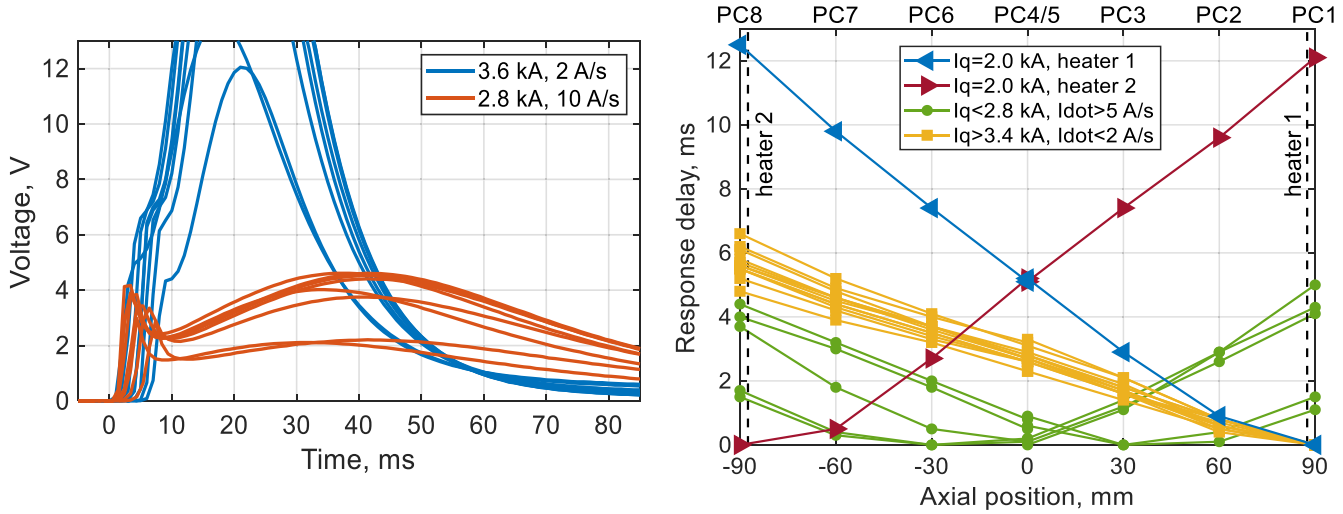

Figure 17. Left: voltage of the pickup coils versus time during the coil quenches at 3.6 kA and 2.8 kA. Right: delay time of response among the pickup coils for the quenches deliberately triggered by heaters at 2.0 kA and spontaneous quenches at higher currents.

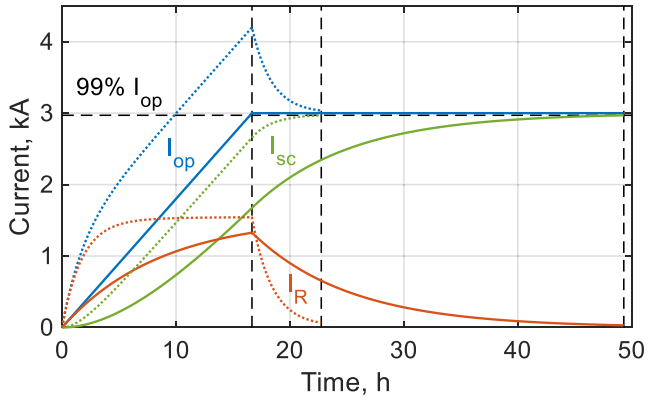

Figure 18. Regular (solid lines) and overshoot (dotted) charging of a coil with time constant ≈ 9 h.

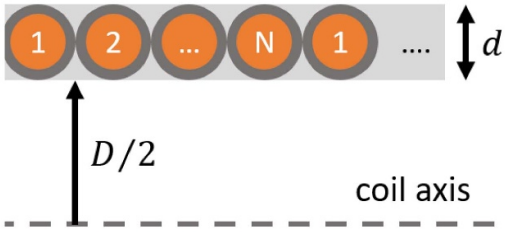

Figure 19. N parallel conductors in a single layer soldered solenoid.

significant reduction of the total charging time, up to 50%, can be achieved by operating the total current as follows:

$$I(t) = \begin{cases} \alpha t + A\left(1 - e^{-t/\beta}\right), t < t_0 \\ I_0 + Ae^{-\frac{t-t_0}{\beta}}, t \geq t_0 \end{cases} \quad (3)$$

where A is the value of overshoot and β an arbitrary time constant, typically ≈ 0.2 τ. A comparison between a regular charging and an overshoot charging is given in figure 18, where the total current and its sharing among the superconductor and transverse resistance are shown as a function of time.

In this particular example, a coil of 1 m diameter and 3 m length is considered. For the conductor described in section 2, it results in a 3 H self-inductance and 100 $\mu\Omega$ transverse resistance, thus a time constant of 8.6 h (note $\sim D^3$ scaling in the equation (1)). Charging such a coil to 3 kA corresponds to 3 T generated magnetic field and 13 MJ stored energy. It would take about 49 h using a regular ramp following equation (2), against 23 h if the overshoot method by 40% is used in accordance with equation (3). The faster charging is due to higher voltage applied over the coil terminals, which is proportional to the current through the transverse resistance.

Note that the current through the transverse resistance saturates towards the same value $\alpha\tau$ for both options and the current in the superconductor never exceeds the target current I_0. Hence, the coil's mechanical stress is not increased, while a trade-off between enhanced cryogenic load due to current leads and decreased static load following the shorter operation has to be resolved.

Using N parallel conductors within the layer allows to reduce the time constant by N^2, similar to the results presented for the ReBCO pancake coils in [17]. As illustrated in figure 19, the soldered strands are fully transposed and should share the transport current uniformly. Compared to the same winding geometry performed by a single strand, the transverse resistance is unchanged, the operating current is increased by a factor N, and thus the self-inductance is reduced by N^2. For the example considered above, the time constant of 8.6 h for a single strand winding will be reduced to 0.5 h by using four parallel strands. The required operation at about 8 kA instead of 2 kA is rather typical for magnets of ∼10 MJ stored energy.

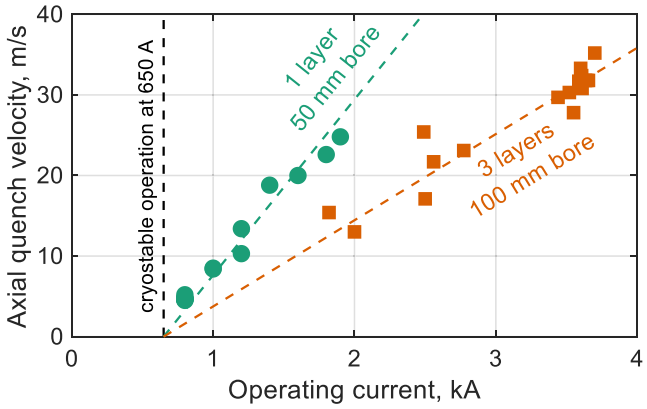

Figure 20. Axial quench propagation velocity versus operating current for the single layer and three layer solenoids. Linear guides are shown starting from 650 A, at which cryo-stable operation of the first coil has been observed.

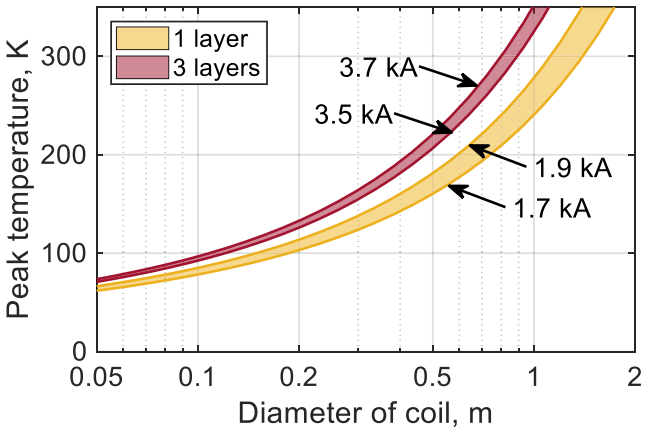

Figure 21. Peak temperature in self-dumped soldered-turns solenoids with varying diameter.

Using the data presented in figures 10 and 17, the quench propagation velocity along the axial direction of the two tested coils was calculated and summarized in figure 20. It is up to 25 m s^{-1} at 1.9 kA operation for the first coil and up to 35 m s^{-1} at 3.7 kA for the second one. These values cannot be directly compared to the normal zone propagation velocity along the wire because of the dominant transverse propagation effect among the winding turns. If the quench propagation in the coils is only assumed along the conductor, it would correspond to the unrealistic numbers of 4 km s^{-1} at 1.9 kA and 11 km s^{-1} at 3.7 kA, i.e. scaled by π D/d.

As mentioned previously, it was possible to recover the fully quenched first coil by decreasing the operating current to 650 A. When considering this as a 'cryo-stable' operation, it can be compared to Stekly's criterion for cryostability:

$$\rho_l j^2 S = qP \rightarrow I = \sqrt{\frac{qPS}{\rho_l}} \approx 540A, \tag{4}$$

where ρ_l is the longitudinal resistivity estimated for copper as 85 nΩ.mm, P = π d the wetted perimeter, S = π $d^2/4$ the conductor cross-section and q the cooling power taken as 10 mW mm^{-2}.

The axial quench velocity, equal to zero at the point of cryostability, scales almost linearly with the operating current, with a twice higher slope obtained for the first coil. Under adiabatic assumptions, the transverse quench propagation velocity can be roughly estimated as $\sqrt{k_\perp/k_l V}$, where k is the heat conductivity and V the normal zone propagation velocity along the wire [12]. The transverse heat conductivity is about 2.5 W/m/K, which is obtained using the Wiedemann–Franz law and the transverse resistivity of 100 nΩ.m. It results in 20 m s^{-1} for the transverse velocity in the single layer coil operated at 1.9 kA ($k_l \approx$ 1200 W/m/K, V $\approx$ 400 m/s), which is nicely validating the assumptions. However, the same analysis applied to the second coil yields only some 10 m s^{-1} at 3.7 kA, clearly underestimating the measured value. Therefore, it is necessary to account for strong electromagnetic coupling among the layers to property evaluate the quench propagation process.

Based on the obtained performance of the soldered-turns coils, one can estimate the peak temperature during the quench assuming that the entire coil volume turns into the normal state instantaneously and cooling terms can be neglected. Therefore, the temperature rise from the initial value T_0 up to T_{max} is calculated simply as follows:

$$m \int_{T_0}^{T_{max}} c\,(T)\,dT = E, \tag{5}$$

where E is the stored magnet energy, m total mass of the conductor and c its effective heat capacity. The temperature increases up to about 60 K for the first coil operated at 1.7 kA and up to 90 K for the second coil at 3.5 kA, corresponding to an energy/mass ratio of 3 and 9 kJ kg^{-1}, respectively. As shown in figure 21, further increasing the coil diameter strongly affects the peak temperature. This is caused by the magnet's stored energy increasing faster with the diameter since proportional with D^2, than the conductor mass proportional with D, leading to the ratio E/m of 100 kJ kg^{-1} at a 1 m bore diameter. Hence, the soldered-turns solenoids can only be considered self-protected for diameters smaller than about 1 meter and would require active protection for larger size.

Mechanical stress increases also rapidly for coils of larger size. The hoop stress scales as $\sim B^2$ D/W, where W is the winding thickness. It is some 50 MPa in the single-layer coil producing 2.0 T and some 250 MPa for the three-layer coil producing 3.8 T. Hence, in contrast to these two coils, a proper additional support structure becomes necessary if higher magnetic field and/or larger diameters are of interest.

Detector magnets are often thin solenoids of large diameter, larger than 1 m, generating relatively low magnetic fields of 2 to 3 T but still with high stored energies of more than 10 MJ [18]. As a consequence, the operating current density is normally less than 50 A mm^{-2}, which is required to contain the hot-spot temperature within limits. The magnets are commonly operated in stationary mode. High operating current densities of up to 1000 A mm^{-2} have been achieved on model detector coils at LBNL in the late 70's enabled by advanced protection circuits providing fast discharge in

less than 0.1 s [19]. Although this technology has been used in some experiments at that time, its scaling towards higher stored energies was found challenging, thus it was mostly abandoned in a favor of Al-stabilized conductor windings.

Soldered-turns solenoids can be an appealing solution for some detector magnets. In particular considering radiation length as they feature 0.07 for a single layer coil and 0.18 for a three closely-packed layer coil. Their ability for stationary operation up to 1900 A mm^{-2} at 2 T and 1300 A mm^{-2} at 4 T is demonstrated, but at relatively small scale.

6. Conclusion

Two demonstrator solenoids, a single-layer on 50 mm bore and three layers on 100 mm bore, with fully soldered windings were manufactured using NbTi/Cu wire with CuNi cladding of 1 mm diameter. From the coil test measurements performed in liquid helium, the salient findings can be outlined as follows:

a. The coils are free from any training, reaching stationary operation at 104% and 96% of the expected performance according the wire critical current;
b. The performance of the coils have met the design values. The generated magnetic field is up to 2.3 T at 2.0 kA and 3.8 T at 3.7 kA, while the time constants are 5 s and 55 s, and the self-inductances are 0.5 mH and 1.7 mH for the first and second solenoids, respectively. The stationary operating current densities of respectively 1900 A mm^{-2} and 1300 A mm^{-2} were achieved.
c. The coils are self-protected within the entire range of operating currents. It takes less than 100 ms for the coils to completely transition to normal state. Thermal runaway is not present even when the operating current is kept constant during the quench. Furthermore, the first coil self-recovers after a quench at relatively low operating currents up to 800 A.

The manufacturing process of the soldered turns NbTi/Cu/Cu30Ni coils is simple as long as insulation is not necessary to reduce the time constant. Hence, in order to scale the process towards larger coil sizes, soldering techniques effective at large-scale needs development. In addition, solenoids of about 1 m diameter or larger require additional support structure and active quench protection. Nonetheless, when compared to large bore detector solenoids, where aluminum stabilized cables are typically used and quench protection is still challenging, the cost and complexity of manufacturing might be greatly reduced by using the proposed magnet design for certain detectors.

Soldering of the turns in the winding layers may also be beneficial for stationary magnets aiming at transverse magnetic fields, such as those based on canted windings. However, the winding layers need to be insulated from each other, thus a higher manufacturing complexity has to be addressed.

Acknowledgments

The authors thank David Frost from SuperCon for the provided technical data and pictures concerning the NbTi/Cu/Cu30Ni conductor, Igor Titenkov and Anton Titenkov for constructing the two solenoids, as well as Torsten Koettig and Laetitia Dufay-Chanat from the Cryolab at CERN for organizing the measurements in liquid helium.

ORCID iDs

N Bykovskiy https://orcid.org/0000-0003-2009-3112
A Dudarev https://orcid.org/0000-0002-8713-8162
M Mentink https://orcid.org/0000-0001-9769-0578
H H J ten Kate https://orcid.org/0000-0001-5597-3190

References

[1] Yamamoto A and Taylor T 2012 Superconducting magnets for particle detectors and fusion devices *Rev. Accel. Sci. Technol.* **05** 91–118
[2] Dudarev A V, Keilin V E, Kuroedov Y D, Konjukhov A A and Vysotsky V S 1995 Quench protection of very large superconducting magnets *IEEE Trans. Appl. Supercond.* **5** 2 226–9
[3] Lubell M S 1972 State-of-the-art of superconducting magnets *Cryogenics* **12** 340–55
[4] Yamamoto A *et al* 2008 The ATLAS central solenoid *Nucl. Instrum. Methods Phys. Res.* A **584** 53–74
[5] Schael S *et al* 2019 AMS-100: the next generation magnetic spectrometer in space – an international science platform for physics and astrophysics at Lagrange point 2 *Nucl. Instrum. Methods Phys. Res.* A **944** 162561
[6] Dudarev A V, Gavrilin A V, Ilyin Y A, Keilin V E and Kopeikin N P 1997 Superconducting windings with 'short-circuited' turns *Inst. Phys. Conf. Ser.* **158** 1615–8
[7] Hahn S, Park D K, Bascunan J and Iwasa Y 2011 HTS pancake coils without turn-to-turn insulation *IEEE Trans. Appl. Supercond.* **21** 1592–5
[8] Suetomi Y, Takahashi S, Takao T, Maeda H and Yanagisawa Y 2019 A novel winding method for a no-insulation layer-wound REBCO coil to provide a short magnetic field delay and self-protect characteristics *Supercond. Sci. Technol.* **32** 045003
[9] Hahn S, Park D K, Kim K, Bascunan J and Iwasa Y 2012 No-insulation (NI) winding technique for premature-Quench-free NbTi MRI magnets *IEEE Trans. Appl. Supercond.* **22** 4501004–4501004
[10] Kim Y *et al* 2014 Partial-insulation winding technique for NbTi coils *IEEE Trans. Appl. Supercond.* **24** 1–5
[11] Noguchi S, Monma K, Itoh R and Igarashi H 2015 Numerical electromagnetic simulation of effective partial-insulation NbTi superconducting coil *Phys. Procedia* **65** 233–6
[12] Wilson M N 1983 *Superconducting Magnets* (Oxford: Clarendon)
[13] Boutboul T, Le Naour S, Leroy D, Oberli L and Previtali V 2006 critical current density in superconducting Nb-Ti strands in the 100 mT to 11 T applied field range *IEEE Trans. Appl. Supercond.* **16** 1184–7
[14] Bottura L 2000 A practical fit for the critical surface of NbTi *IEEE Trans. Appl. Supercond.* **10** 1054–7
[15] Wang Y, Song H, Yuan W, Jin Z and Hong Z 2017 Ramping turn-to-turn loss and magnetization loss of a No-Insulation

(RE)Ba2Cu3Ox high temperature superconductor pancake coil *J. Phys. D: Appl. Phys.* **121** 113903

[16] Kim S, Hahn S, Kim K and Larbalestier D 2017 Method for generating linear current-field characteristics and eliminating charging delay in no-insulation superconducting magnets *Supercond. Sci. Technol.* **30** 035020

[17] Geng J and Zhang M 2019 A parallel co-wound no-insulation REBCO pancake coil for improving charging delays *Supercond. Sci. Technol.* **32** 084002

[18] Green M A 2017 The development of superconducting detector magnets from 1965 to the present *IEEE Trans. Appl. Supercond.* **vol. 27** 1–8

[19] Taylor J*et al*1979Quench protection for a 2-MJ magnet*IEEE Trans. Magn.* **15**855–9